

Surrogate Markers for Glioma Diagnosis: Diffusion Weighted Magnetic Resonance Imaging and Magnetic Resonance Spectroscopy

April 7, 2009

Lars Ewell, Amarjeet Bhullar, Ray Carmody,
Russell Hamilton, Joshua Kim and Baldassarre Stea

Abstract

A series of surrogate markers are proposed that will investigate the ability to predict efficacy of radiation therapy for primary or metastatic gliomas. The Apparent Diffusion Coefficient (ADC), obtained from Diffusion Weighted Magnetic Resonance Imaging (DWMRI), along with Magnetic Resonance Spectroscopy (MRS) are both probed for their predictive ability.

Introduction

The goal of a surrogate marker that can predict efficacy of radiation therapy remains elusive. Such a marker could, in principal, allow for informed clinical decisions on therapeutic patient care, thereby increasing the quality of life for the patient under treatment. A number of promising potential candidates will be examined, primarily consisting of the Apparent Diffusion Coefficient (ADC), determined from Diffusion Weighted Magnetic Resonance Imaging (DWMRI), and Magnetic Resonance Spectroscopy (MRS). Due in part to lack of motion artifacts, the brain lends itself to these types of imaging modalities.

The ADC has been shown to have potential to predict whether or not tumors are responding to cytotoxic therapies [1, 2]. In addition, the ADC has also been utilized in an attempt to differentiate radiation necrosis from recurrent disease in gliomas both by itself [3], and in conjunction with MRS [4]. Each of these complimentary imaging modalities will be investigated for monitoring efficacy, as well as differential diagnosis (necrosis vs. recurrent disease).

Specific Aims

Lesion Volume/Location

An important criteria when considering diagnosis and/or therapy for gliomas are the size and location of the lesion. The lesion size is known to be inversely correlated with survival, with tumors (GBM) larger than 5cm having a poorer prognosis ($p=0.04$) [5].

While lesion location has yielded less predictive information, there has been recent speculation that tumors situated adjacent to the lateral ventricles have a poorer prognosis [6]. Regardless of whether or not these prognostic suspicions are true, the location does have an important role in determining how easily the lesion can be probed, e.g., with MRS [7]. In addition to affecting MRS, lesion location can also influence the accuracy with which ADCs can be calculated. e.g., in the cerebrum, the sulci density can impact the value of the ADC derived from DWMRI scans [8].

In view of these facts, in this study we propose to undertake we will record as accurately as possible, the size and location of the lesions being treated with radiotherapy in our department. This information is of ultimate importance, as it will allow for differences to be quantified. The question of whether or not the lesion is resected is also central to this study (see below).

MRS Spectra and DWMRI Scans

For the patients enrolled, DWMRI scans as well as MRS scans will be obtained. After the initial clinical scans have taken place, and it is determined that the patient is eligible to enroll (see criteria below), the patient will undergo three multivoxel MRS scans, one coincident with the lesion, one inferior and one superior. The slice thickness will be one cm and the voxel size will be 2x2cm. Figure 1 shows a sample of the 7x7 multivoxel MRS grid superimposed on an MRI scan.

Quantify Tumor Response

Of paramount importance when attempting to evaluate surrogate markers is the ability to quantify how the tumor reacts, if at all, to radiation therapy. For this study, the primary end-point is objective tumor response. For solid tumors not in the brain, the Response Evaluation Criteria In Solid Tumors (RECIST) is often used to quantify tumor response [9]. However, the brain has different criteria due in part, to the ethical problems involved with obtaining 'margins' from grossly intact white matter [10], as well as the blood brain barrier. For this reason, we will adhere to the criteria developed in an earlier study [11].

Unresected

If the tumor, for whatever reason, is not resected/debulked, then the dimensions are more straightforward to obtain. As indicated in this previous work, the *size* of the tumor is considered as the largest cross-sectional area on a contrast enhanced T1 weighted MRI scan[11]. Once the

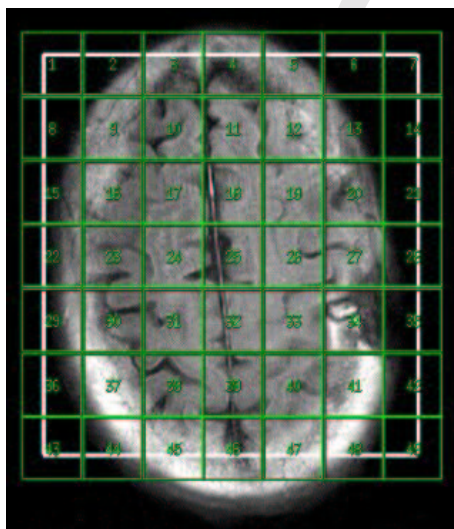


Figure 1: MRS Grid.

size has been determined, the tumor will be monitored longitudinally during which time it will be categorized according to its' response (if any) to radiation therapy. These criteria are listed in Table 1:

Resected/Debulked

It is expected that the majority of patients enrolled in this study will be candidates for resection. This substantially complicates the determination of lesion size. e.g., if the tumor is successfully removed, in principal there should be no enhancing lesion left to quantify/monitor. Figure 2 shows such a situation. If, as in this figure, the lesion (frontal lobe, patient right, hypo-intense) has been successfully resected, the surrounding intact white matter will be longitudinally monitored for recurrence. It is also possible that an area around the initial enhancing lesion remains after resection. This is shown in Figure 3. As can be seen here, there remains a small enhancing lesion (frontal lobe, posterior to hypo-intense cavity) that can and will be longitudinally monitored.

Pseudoprogression

A confounding factor in regards to objectively quantifying tumor response is the so called phenomena of *pseudoprogression* [12]. Pseudoprogression can be characterized as an exaggerated response to effective therapy. i.e. although the lesion may appear to grow on a 'normal' T1-weighted contrast enhanced MRI, the growth is actually false, and the patient is in fact responding to therapy. This has the potential to, e.g., increase the number of patients categorized as PD and/or SD, while decreasing the number of patients categorized as CR and/or PR(see Table 1). We will attempt to remain aware of the possibility of this occurring, and act accordingly.

Table 1: Response Criteria for Registered Lesions

Complete Response (CR)	Disappearance of all enhancing lesion on consecutive MRI scans at least one month apart, off steroids and neurologically stable or improved.
Partial Response (PR)	$\geq 50\%$ reduction in size of enhancing lesion on consecutive MRI scans at least one month apart, steroids stable or reduced and neurologically stable or improved.
Progressive Disease (PD)	$\geq 25\%$ increase in size of enhancing lesion on consecutive MRI scans, or neurologically worse and steroids stable or increased.
Stable Disease (SD)	All other situations.

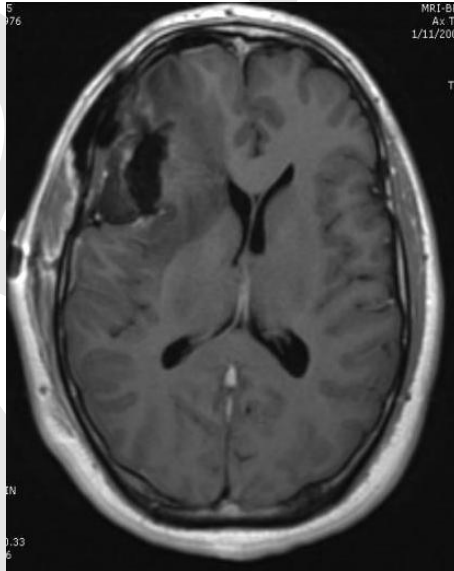


Figure 2: Glioma successfully resected.

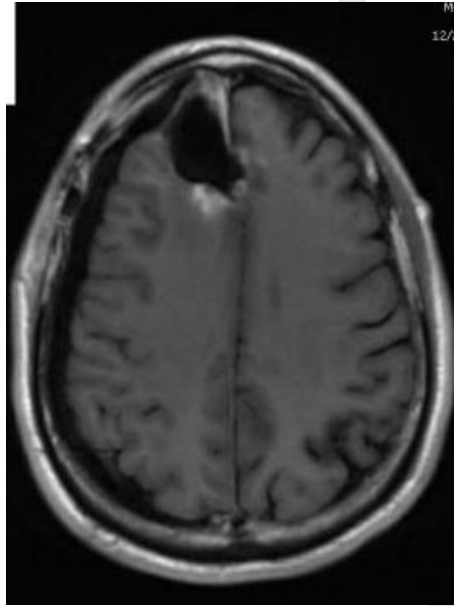


Figure 3: Glioma resected with small enhancing lesion remaining.

Radiation Necrosis vs. Recurrent Disease

In addition to quantifying tumor response to radiation therapy, an important diagnostic consideration regarding gliomas is the ability to differentiate radiation necrosis from recurrent disease. In a typical T1 weighted MRI scan, both radiation necrosis (a side effect from radiation) and recurrent disease can appear as 'enhancing lesions' (hyperintense region) [13]. In view of this fact, we will monitor all areas of the brain that receive enough radiation to have a *reasonable*(between 5% and 24%[13]) chance to suffer from radiation necrosis.

Background and Significance

Previous use of ADC: Treatment Efficacy

As indicated above, the ADC has been used to monitor cancer treatment efficacy, including both chemotherapy and radiation therapy. Diffusion weighting the MRI sensitizes the scan to mobility of H_2O . It is hypothesized that as effective cytotoxic cancer therapy progresses, cellular breakdown of the tumor occurs, thereby allowing H_2O to move more easily in and around the disease site. Since necrotic tissue, cancerous or otherwise, is thought to undergo cellular breakdown leading to increased water mobility, it has been suggested that DWMRI could also be useful in discriminating between Radiation Induced Necrosis (RIN) and recurrent disease.

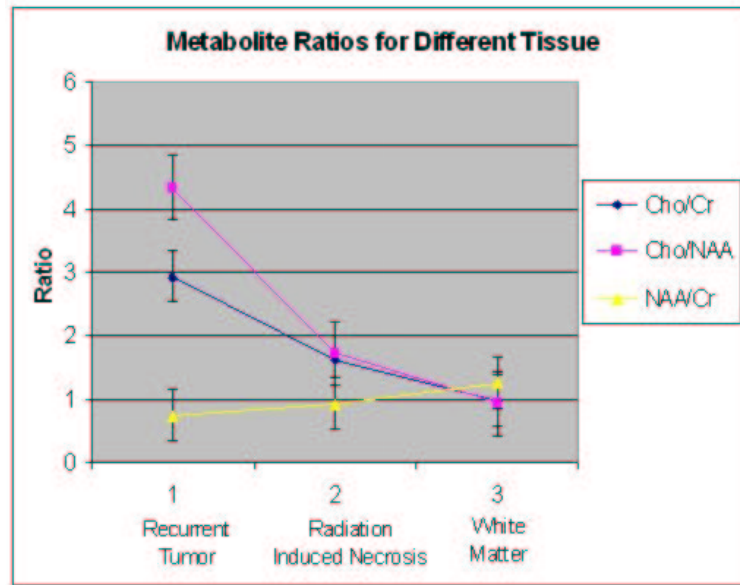


Figure 4: Metabolite ratios of recurrent disease, RIN and normal white matter.

Previous use of MRS: Differential Diagnosis

MRS, also known as Chemical Shift Imaging (CSI), has proven useful in discriminating between RIN and recurrent disease. It can determine metabolite levels, the ratios of which have the potential ability to differentiate RIN and recurrent disease. MRS obtains its signal from the shift in the MR signal due to the surrounding chemical environment [14]. Regarding the brain, three of the main metabolites of interest are: 1) Choline (Cho) a neurotransmitter that is increased in tumors. 2) N-Acetyl Aspartate (NAA) a neuronal metabolite that is decreased in tumors. 3) Creatin (Cr), a brain metabolite. Figure 4 shows a plot of the potential discriminating power of metabolite ratios from some previous work [7].

Apoptosis/Mitosis

The two primary mechanisms of clonogenic cell death following irradiation are mitotic death and apoptosis[21]. Mitotic death, which occurs when cells fail to divide because of damaged or lost chromosomal material or the failure of spindle formation during cytokinesis, is the most common mechanism. One or more cell divisions may occur prior to cell death. Apoptosis prevalence depends strongly on the tumor type and occurs without cell division.

The expected ADC signal is significantly different for mitotic and apoptotic death. Cells undergoing mitotic death increase their size, for example when giant cells with multiple nuclei form. The ADC is expected to decrease during this process since the intercellular spacing and fluid are reduced. Then these cells become necrotic and their membranes are compromised, resulting in excess intercellular fluid and expected increases in water mobility and the ADC.

The duration of this process depends on the cell cycle time since cells undergo one or more cell divisions before dying. This would be considered a delayed response to radiation as it would occur days after exposure. In apoptotic death, the cell detaches from its neighbors, chromatin condenses at the nuclear membrane, cytoplasmic condensation causes the cell to shrink, and water is lost. An increase in ADC is expected to occur [15]. Next, these cells become necrotic and are then phagocytized. During these processes, the ADC is expected to be larger than prior to irradiation. Apoptosis occurs within 4 to 24 hours following exposure. Finally, for either mechanism, the tissue in the irradiated volume must reorganize. The ADC in this region may be larger or smaller than in the pretreatment scan, depending on whether tumor or normal cells occupy this volume and their density within it.

Preliminary Studies

MRS

As part of a related Internal Review Board (IRB) approved study¹, a number of patients as well as an MRS phantom have been scanned using multi-voxel MRS. The spherical MRS phantom (diam=20.3cm) contained the three brain metabolites, Cho, Cr and NAA in roughly the same concentrations as a healthy human brain: 3.0 milli-molar(mM), 10.0mM and 12.5mM respectively. The metabolite peaks were fit using a Gaussian function, and the metabolite concentrations and ratios were plotted as a function of voxel location. Figure 5 depicts the phantom with the 7x7 grid superimposed, as well as a sample spectra from voxel 25. The

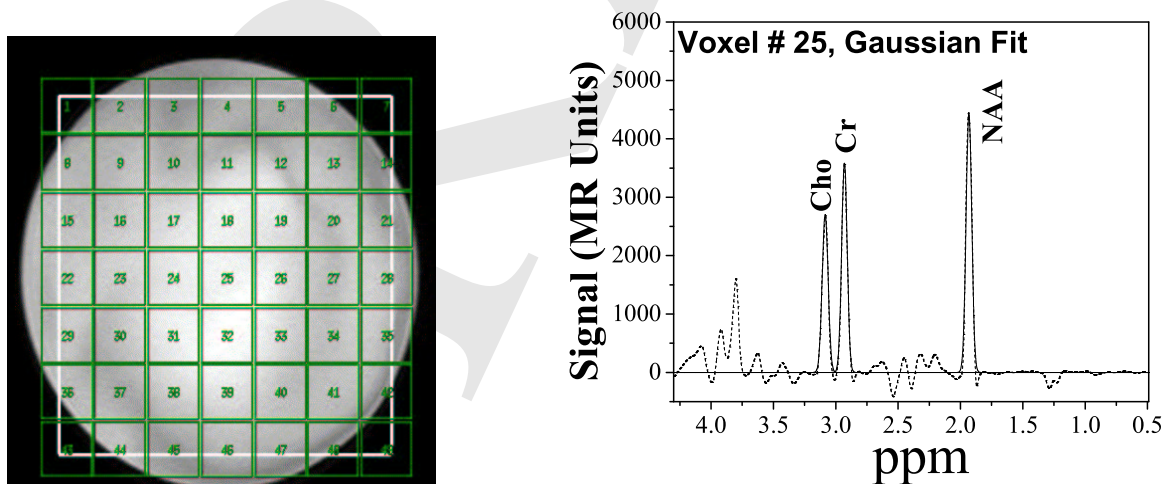


Fig 5: **Left** - An MRI image of the CSI phantom filled with Cho(3.0mM), Cr(10.0mM), and NAA(12.5mM) and a 7x7 grid superimposed.; **Right** - The spectra from voxel number 25. The dashed line is the real spectrum and solid line as Gaussian functions overlapped on respective peaks.

¹see <http://www.u.arizona.edu/lewell/protocol/index.html>

Table 2: Phantom Metabolite Concentration and Ratio Variation

Metabolite-Ratio	Min	Mean	Max	% Variation
Cho	52.7	96.3	159.6	202
NAA	79.4	146.7	250.0	215
Cho/NAA	0.61	0.63	0.67	9.0

data from these spectra are displayed in Table 2. As can be seen there, although the MRS signal (peak area) for Cho and NAA for different voxels varies by 202 and 215% respectively, the Cho/NAA ratio is constant to within 9%, indicating that the metabolite ratio is relatively insensitive to MRS signal fluctuations. Figure 6 depicts the absolute metabolite fluctuation, as well as the ratio variation as a function of voxel location. Only the central 25 voxels were analyzed. As can be seen in this figure, the absolute metabolite signal (peak area) showed a

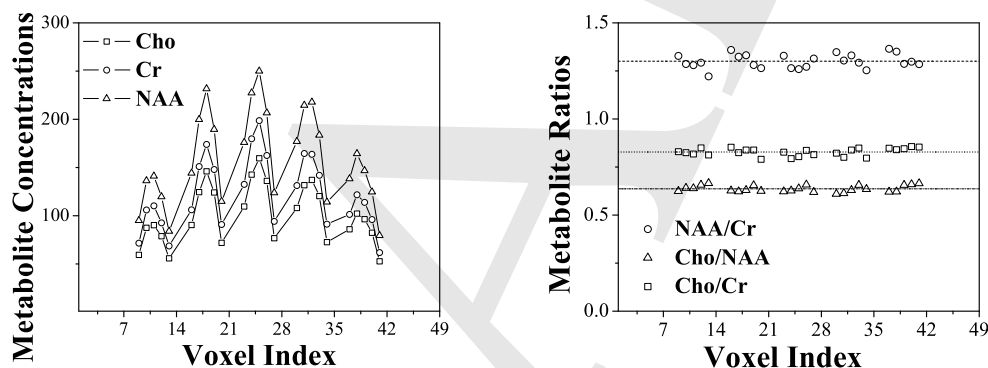


Figure 6: **Left** - Absolute metabolite concentration (peak area) as a function of voxel location. Central voxel (25) has highest concentration. **Right** - Metabolite ratio as a function of voxel location.

significant correlation with voxel location, whereas the ratio did not.

For this MRS phantom, our metabolite calculations were in good agreement with the automatic ratios that are calculated via the *Functool* software on the 3T GE Excite MRI machine. However, for patients, the variation in metabolite ratio and peak location was much less predictable. For this reason, we display the MRS data in this form, so as to more accurately represent the ratios. In Figure 7, a healthy volunteer MRS spectra is displayed. In Figure 8, a patient MRS scan is displayed. These data are also displayed in Table 3, similar to Table 2. As can be seen in these data, the volunteer and patient absolute metabolite signals show a variation similar to the phantom. However, the volunteer and especially the patient Cho/NAA ratio exhibits far more variation than the phantom data. In addition to the ratio variation, the background of patient scans add a level of complexity to MRS interpretation. In Figure 9 a patient MRS scan is displayed, along with background. As can be seen in this spectra, a large (lipid/lactate) peak adds substantially to the background. To estimate the background, some anchor points are chosen that presumably lie outside the range of the known MRS peaks(left

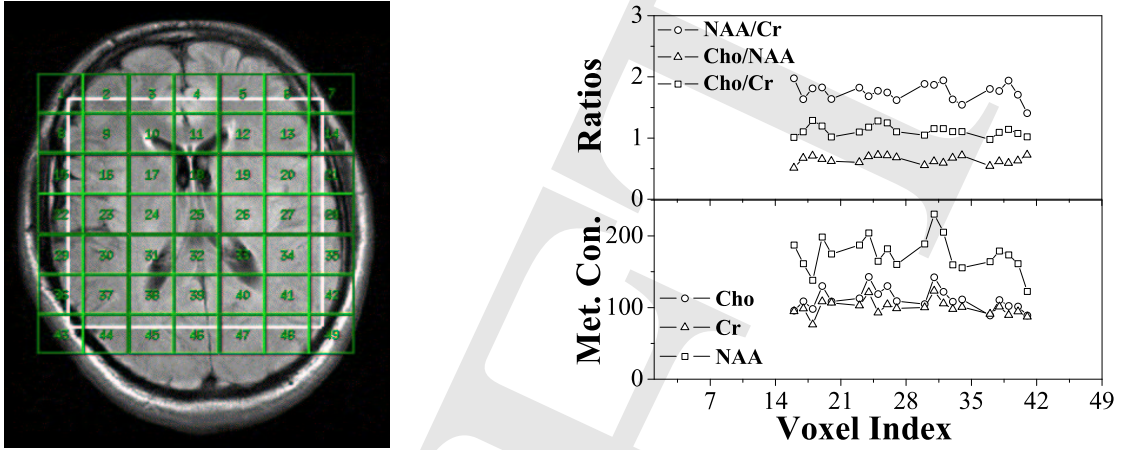


Figure 7: **Left** - Healthy Volunteer MRS scan. **Right** - Metabolite and ratio variation.

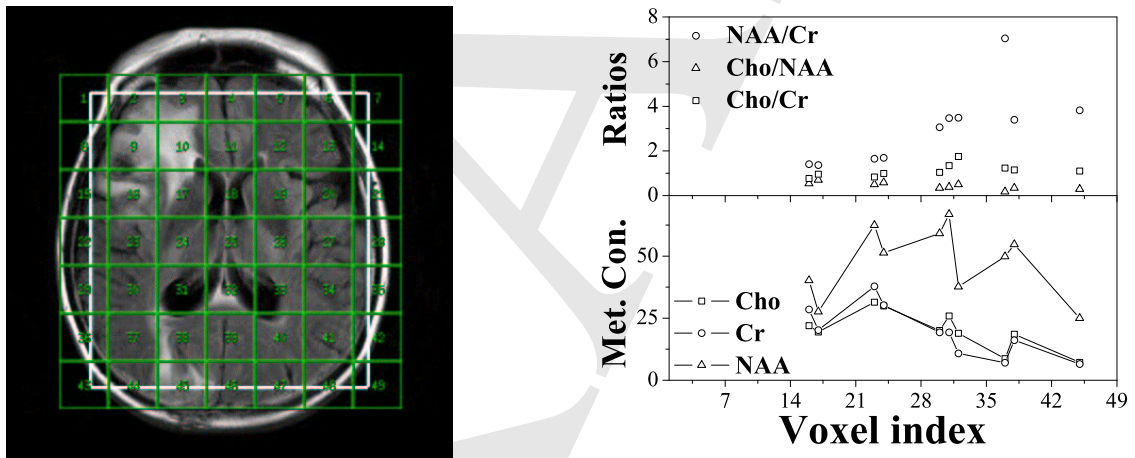


Figure 8: **Left** - Patient MRS scan. **Right** - Metabolite and ratio variation.

Table 3: Patient and Volunteer Metabolite Concentration and Ratio Variation

Person	Metabolite/Ratio	Min	Mean	Max	% Variation
Volunteer	Cho	88.9	111.8	142.8	60.6
Volunteer	NAA	122.6	174.1	230.5	88.0
Volunteer	Cho/NAA	0.51	0.64	0.73	43.1
Patient	Cho	7.20	19.73	31.42	336
Patient	NAA	25.01	50.57	66.88	167
Patient	Cho/NAA	0.18	0.44	0.70	300

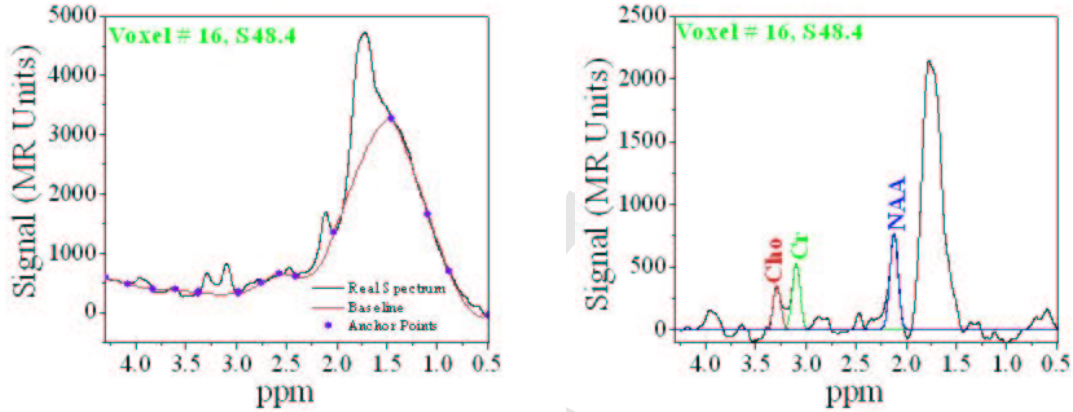


Figure 9: **Left** - Voxel spectra with background(lipid). **Right** - Voxel spectra with background subtracted.

plot). The background is then subtracted, to yield a spectra that is more easily analyzed(right).

ADC

In addition to the MRS scans mentioned above, the same patients also received isotropic Diffusion Weighted MRI (DWMRI) scans as a part of the imaging protocol. These included two different types of diffusion weighting: 1) The most common form of diffusion weighting, echo planar [16]. 2) A more recently developed form of diffusion weighting, radial diffusion [17]. In Figure 10, the lesions of an enrolled patient are displayed. These lesions were longitudinally

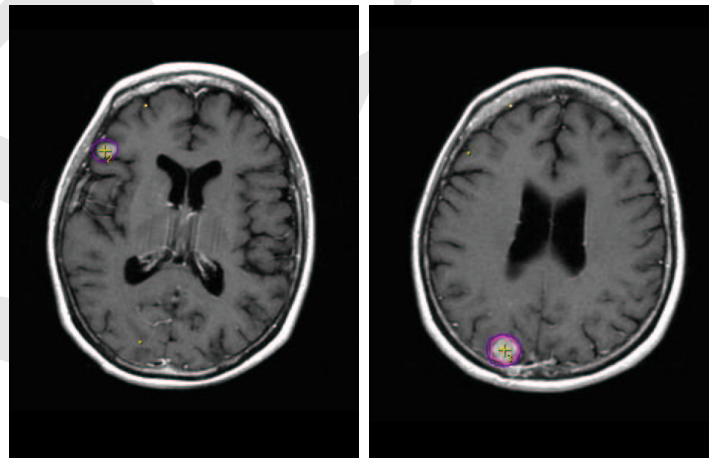


Figure 10: **Left** - Lesion number 2. **Right** - Lesion number 3.

monitored, using both echo planar and radial diffusion DWMRI scans. Some of the characteristics of the different types of DWMRI scans are displayed in Table 4. The ADC is determined

Table 4: DWMRI Scan Characteristics

Scan Type	b-values(s/mm ²)	Slice Spacing(mm)	Slice Thickness(mm)
Echo Planar	0, 1000	7	5
Radical Diffusion	0, 520, 850	7	5

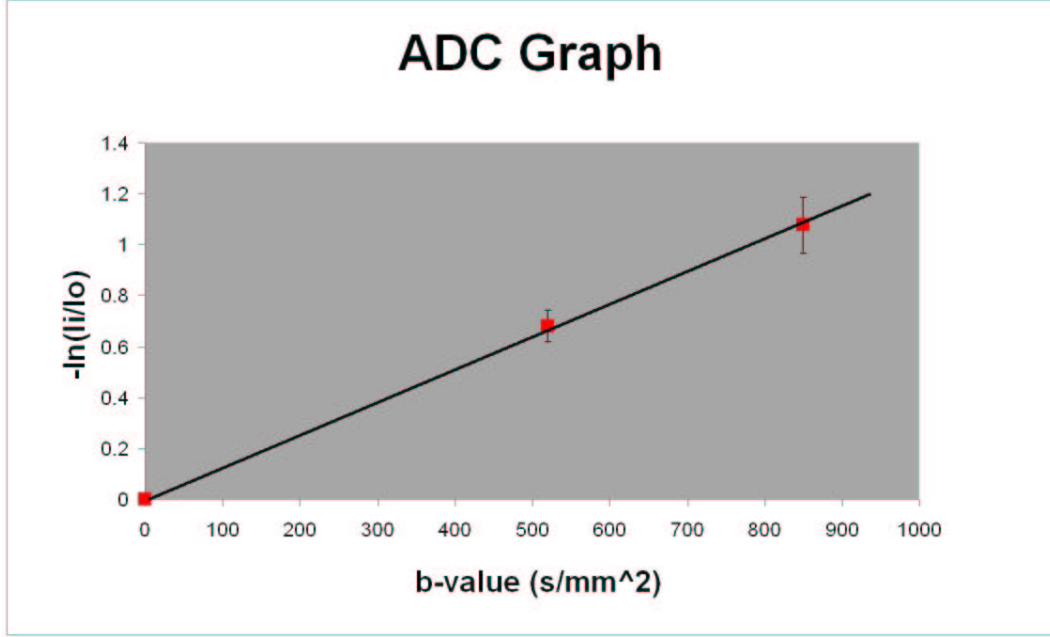


Figure 11: Plot used to determine ADC and Statistical Uncertainty.

via a plot of the ratio of the log of pixel intensities vs. b-value:

$$\log \frac{I_i}{I_o} = -b_i * ADC \quad (1)$$

where i represents the different b-values of diffusion weighting, and I_i is the corresponding pixel intensities of the lesions in these scans. Error bars are calculated to accommodate the transcription uncertainty, as well as noise [18]. After this uncertainty is quantified, this equation is plotted. A typical plot is shown in Figure 11. As can be seen, the $b=0$ ($i=0$) point has no error bars since in the fraction, the numerator equals the denominator: I_o . Furthermore, since $\log(1) = 0$, there is no intercept. Previous work has demonstrated the importance of uncertainty in the highest b-value [19]. A weighted least squares fit to the data is performed [20], the slope of which is the ADC:

$$ADC = \frac{1}{\Delta} \left(\sum_{i=0}^n \frac{b_i}{\sigma_i^2} \log \frac{I_i}{I_o} \right) \quad (2)$$

with

$$\Delta = \sum_{i=0}^n \frac{b_i^2}{\sigma_i^2} \quad (3)$$

where σ_i are the total systematic uncertainties associated with the different log ratios determined above and i ranges over the different b -values of diffusion weighting. Finally, the total (systematic + statistical) uncertainty in the ADC can be written

$$\sigma_{ADC}^2 = 1 / \left(\sum_{i=0}^n \frac{b_i^2}{\sigma_i^2} \right). \quad (4)$$

A plot of the ADC of the two lesions referred to above is shown in Figure 12. As can be seen

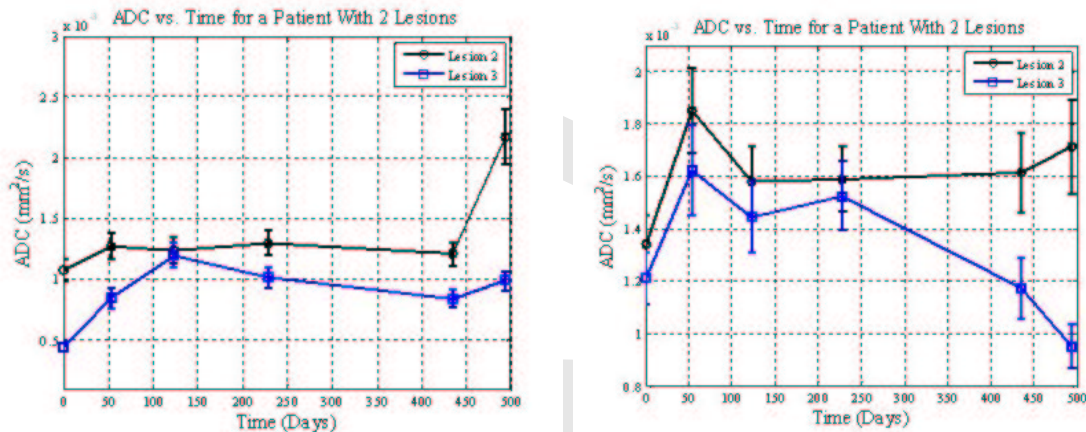


Figure 12: **Left** - Echo Planar ADC vs time. **Right** Radial Diffusion vs time.

in this figure, there is a difference between the two types of diffusion weighting.

Research Design and Methods

Imaging Protocol

Since the majority of gliomas recur within 2cm of the primary [21], we plan on initiating an imaging protocol whereby we will monitor the disease site longitudinally, using both DWMRI and MRS. Multi-voxel MRS with a 7x7 grid size and 2x2x1cm voxels will allow for both the disease itself to be monitored, along with contra-lateral brain for comparison. Three slices of MRS data will be acquired: One slice centered on the lesion, and a superior and inferior slice. Some of the characteristics of the scans are displayed in Table 5. In Table 6, some details of the actual scans to be performed are displayed.

Sulci Density

Once the data are acquired, we will compute sulci density maps for all patients enrolled. In a previous study[8], the importance of this density in calculating ADC values was emphasized. In Figure 13, a sulci density map of four different patients is displayed. Similar to the ADC values, the sulci density maps will be longitudinally monitored for change. By using two different type

Table 5: Imaging Sequence for Enrolled Patients

Time From End of Radiotherapy (days)	Scans Performed	Comments
-5	CT, MRI, DWMRI, MRS	Baseline scans. Used to plan radiotherapy. CT and MRI registered using BrainScan.
30	MRI, DWMRI, MRS	First scan for comparison. Look for reduction of edema from surgery.
90	MRI, DWMRI, MRS	Second scan for comparison. Potential radiation necrosis and pseudoprogression.
180	MRI, DWMRI, MRS	Second scan for comparison. Potential radiation necrosis and pseudoprogression.
360	MRI, DWMRI, MRS	Second scan for comparison. Potential radiation necrosis and pseudoprogression.

Table 6: Scan Details

Scan Type	Scan Details	Time Echo (TE, ms)	Repetition Time (TR, ms)	Actual Patient Scan Time (min)
DWMRI	T2 Weighted, RFSE Diffusion Weighted, b=0, 500 and 1,000s/mm ²	76	10,000	10
DWMRI	T2 Weighted, Echo Planar Diffusion Weighted, b=0, 500 and 1,000s/mm ²	76	10,000	10
MRS	PRESS, 2D multivoxel 49 Voxels per slice 1cm slice thickness, 3 slices	144	1,500	30

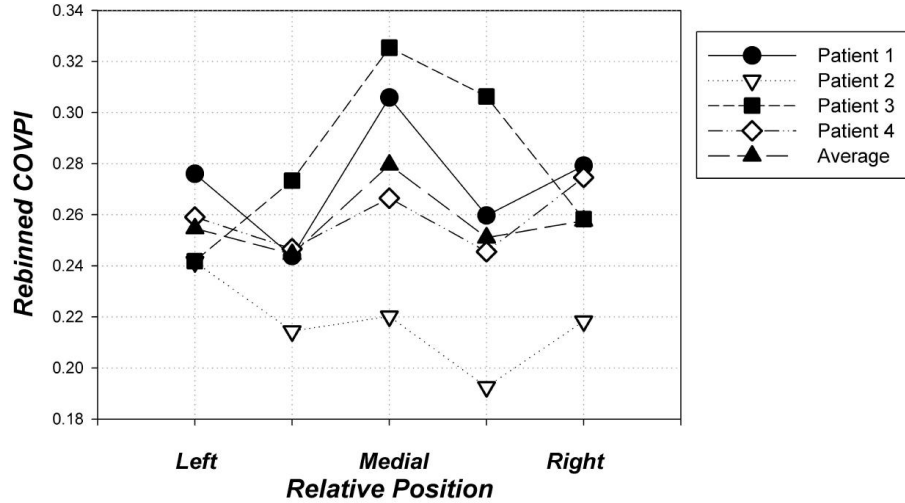


Figure 13: Sulci density map of four patients plotted in the sagittal direction (see reference 8 for details on map calculation).

of isotropic diffusion weighting, as well as sulci density maps, we believe that we will achieve an unprecedented level of accuracy with which to monitor disease sites.

MRS-DWMRI Differences

We expect that DWMRI, particularly using the Radial Fast Spin Echo (RFSE) technique, will have fine resolution (pixel size of 1mm^2 and slice thickness of 3mm). On the other hand the voxel size of the MRS, as indicated in Figure 1, we expect to be on the order of 4cm^3 . This disparity in voxel size has implications about how best to use both of these different imaging modalities. A likely scenario is that tissue within the larger MRS voxel will consist of normal tissue and/or recurrent disease and/or necrotic tumor and/or normal tissue suffering from RIN. How best to differentiate these four different tissue types is one of the main objectives of this study.

Radiation Necrosis/Recurrent Disease

With an α/β ratio of ≈ 2 , normal brain is thought to be a *late* responding tissue regarding therapeutic radiation [22]. For this reason, we do not expect to see evidence of any RIN for months to years after the patients have received therapeutic radiation to the disease site. On the other hand, the tumor is thought to have an α/β ratio of ≈ 10 , and is therefore thought of as an *early* responding tissue regarding therapeutic radiation. For this reason, we expect that we may begin to see reactions of the lesions to radiation in weeks to months after the end of radiation therapy.

Histology Correlation

In the normal course of patient care, histological examinations are common. We realize that the current 'gold standard' for definitive diagnosis of gliomas is a pathologic examination of tissue samples obtained from biopsy. However, in this imaging study, we do not plan on compelling any additional histology, from that which would otherwise be ordered in the absence of this study for the patients that choose to enroll. With this in mind, we will analyze histological data as they become available, and look for statistically significant ($p < 0.05$) correlations between recurrent disease, RIN, ADC value change and/or metabolite ratio change.

Receiver Operating Characteristics

Our ultimate goal in this study is to help facilitate non-invasive definitive diagnosis of gliomas. To this end, we will implement Receiver Operating Characteristics (ROC) to obtain sensitivity and specificity [23] values for MRS and DWMRI as they relate to this diagnosis.

Problems

In a technically demanding study such as this, we expect to encounter a number of problems. One such problem involves the composition of tissue in the Volume Of Interest (VOI). It is likely that many of the regions being probed will include not only pure recurrent disease or pure RIN, but some mixture of the two. This scenario will complicate the ability to draw firm conclusions from any correlations that may be apparent. We will likely have to separate regions into pure disease, pure necrosis and a mixture of the two with the last category most likely containing most of the data points.

An additional problem has to do with VOI placement. We expect that it will be relatively rare that the center of the resection cavity will occur in the middle of a parallelepiped of brain tissue such that the entire VOI will be unobstructed. More likely is the situation that an anatomical feature, such as the skull or the posterior fossa will encroach upon the 588 (49x4x3) cc VOI such that a portion of it will be either obstructed, or have a large susceptibility gradient. We believe that the robustness of the RFSE technique against susceptibility gradients will minimize this problem with respect to the DWMRI scans. The MRS data may be truncated.

References

- [1] Ross BD, Moffat BA, Lawrence TS, Mukherj SK, Gebarski SS, Quint DJ, Johnson TD, Junck L, Robertson PL, Muraszko KM, Dong Q, Meyer CR, Bland PH, McConville P, Hairong G, Rehemtulla A, Chenevert TL. Evaluation of Cancer Therapy Using Diffusion

Magnetic Resonance Imaging., *Molecular Cancer Therapeutics* 2003;2:581-7.

- [2] Theilmann R, Borders R, Trouard TP, Xia G, Outwater E, Ranger-Moore J, Gillies RJ, Stopeck A. Changes in Water Mobility Measured by Diffusion MRI Predict Response of Metastatic Breast Cancer to Chemotherapy. *Neoplasia* 2004;6:831-7.
- [3] Chiaki Asao, Yukunori Korogi, Mika Kitajima, Toshinori Hirai, Yuji Baba, Keishi Makino, Masato Kochi, Shoji Morishita, and Yasuyuki Yamashita, Diffusion-Weighted Imaging of Radiation-Induced Brain Injury for Differentiation from Tumor Recurrence. *AJNR Am J Neuroradiol* 26:1455-1460, June/July 2005.
- [4] QING-SHI ZENG, PH.D.,* CHUAN-FU LI, M.D.,* HONG LIU, PH.D., JUN-HUI ZHEN, M.D., AND DE-CHAO FENG, M.D. DISTINCTION BETWEEN RECURRENT GLIOMA AND RADIATION INJURY USING MAGNETIC RESONANCE SPECTROSCOPY IN COMBINATION WITH DIFFUSION-WEIGHTED IMAGING, *Int. J. Radiation Oncology Biol. Phys.*, Vol. 68, No. 1, pp. 151-158, 2007.
- [5] Barbara Fazeny-Dornera, Catharina Wenzela, Mario Veitlb, Maria Piribauera, Karl Rosslerc, Karin Dieckmannnd, Karl Ungersbockc and Christine Marosia Survival and prognostic factors of patients with unresectable glioblastoma multiforme, *Anti-Cancer Drugs* 2003, 14:305-312.
- [6] Kaisorn L. Chaichana, Matthew J. McGirt, James Frazier, Frank Attenello, Hugo Guerrero-Cazares, Alfredo Quinones-Hinojosa. Relationship of glioblastoma multiforme to the lateral ventricles predicts survival following tumor resection, *J Neurooncol* (2008) 89:219-224.
- [7] P. Weybright, P. Maly, D. Gomez-Hassan, C. Blaesing, P. C. Sundgren. MR spectroscopy in the evaluation of recurrent contrast-enhancing lesions in the posterior fossa after tumor treatment. *Neuroradiology* (2004) 46: 541-549.
- [8] Lars A. Ewell, Christopher J. Watchman, Kurt Wharton, Sulci density map to aid in use of apparent diffusion coefficient for therapy evaluation. *Magnetic Resonance Imaging* 26 (2008) 20-25.
- [9] Patrick Therasse, Susan G. Arbuck, Elizabeth A. Eisenhauer, Jantien Wanders, Richard S. Kaplan, Larry Rubinstein, Jaap Verweij, Martine Van Glabbeke, Allan T. van Oosterom, Michaele C. Christian, Steve G. Gwyther. New Guidelines to Evaluate the Response to Treatment in Solid Tumors, *Journal of the National Cancer Institute*, Vol. 92, No. 3,

February 2, 2000.

- [10] Young G, Advanced MRI of Adult Brain Tumors, *Neurol Clin* 25 (2007) 947-973.
- [11] Macdonald D, Cascino T, Schold SC and Cairncross JG, Response Criteria for Phase II Studies of Supratentorial Malignant Glioma, *Journal of Clinical Oncology*, Vol 8, No 7 (July), 1990: pp 1277-1280.
- [12] Marc C. Chamberlain, Pseudoprogession in Glioblastoma, *JOURNAL OF CLINICAL ONCOLOGY*, VOLUME 26 - NUMBER 26 - SEPTEMBER 10 2008.
- [13] Ashok J. Kumar, Norman E. Leeds, Gregory N. Fuller, Pamela Van Tassel, Moshe H. Maor, Raymond E. Sawaya, Victor A. Levin, Malignant Gliomas: MR Imaging Spectrum of Radiation Therapy- and Chemotherapy-induced Necrosis of the Brain after Treatment. *Radiology* 2000; 217:377-384 .
- [14] Haacke, Brown, Thompson and Venkatesan, *Magnetic Resonance Imaging*, 1999, John Wiley and Sons, Inc., 605 Third Ave., NY, NY 10158-0012.
- [15] Moffat et al., 'Functional diffusion map: A noninvasive MRI biomarker for early stratification of clinical brain tumor response', *Proc. Nat. Ac. Sci.* pp. 5524-5529, 102 no. 15, April 12, 2005.
- [16] Skare S, Rexford D. Newbould, Clayton D, Albers G, Nagle S, Bammer R. Clinical Multishot DW-EPI Through Parallel Imaging With Considerations of Susceptibility, Motion, and Noise., *Magnetic Resonance in Medicine* 57:881-890 (2007).
- [17] Sarlls J, Newbould R, Altbach M, Gmitro A, Seeger J, Trouard T. Isotropic Diffusion Weighting in Radial Fast Spin-Echo Magnetic Resonance Imaging. *Magnetic Resonance in Medicine* 53:1347-1354 (2005).
- [18] Firbank M, Coulthard A, Harrison R, Williams E. A Comparison of Two Methods for Measuring the Signal to Noise Ratio on MR Images. *Phys. Med. Biol.* 44 (1999) N261.N264.
- [19] Vijayakumar N, Ewell L. Relationship of Uncertainty in Pixel Intensity to Apparent Diffusion Coefficient Calculation. SU-FF-I-77, *Medical Physics* 34(6), 2355, June 2007.

- [20] Bevington P. Data Reduction and Error Analysis for the Physical Sciences. New York: McGraw-Hill Inc, 1969.
- [21] Wallner et al., 'Patterns of Failure Following Treatment for Glioblastoma Multiforme and Anaplastic Astrocytoma', International Journal of Radiation Oncology and Biology and Physics, 16, 1405-1409 1989.
- [22] Hall E. J., 'Radiobiology for the Radiologist', Fifth Edition, Lippincott Williams and Wilkins, Philadelphia, PA 2000.
- [23] Motulsky H., 'Intuitive Biostatistics', Oxford University Press, 1995, 198 Madison Avenue, New York, New York, 10016.